The Astrophysical Journal, 716:417–426, 2010 June 10 doi:10.1088/0004-637X/716/1/417
© 2010. The American Astronomical Society. All rights reserved. Printed in the U.S.A.

THERMAL INFRARED MMTAO OBSERVATIONS OF THE HR 8799 PLANETARY SYSTEM*

Philip M. Hinz[1], Timothy J. Rodigas[1], Matthew A. Kenworthy[1], Suresh Sivanandam[1], Aren N. Heinze[2], Eric E. Mamajek[3], and Michael R. Meyer[1,4]
[1] Steward Observatory, The University of Arizona, 933 N. Cherry Ave., Tucson, AZ 85721, USA; phinz@as.arizona.edu
[2] Department of Physics and Astronomy, Swarthmore College, Swarthmore, PA 19081, USA
[3] University of Rochester, Department of Physics & Astronomy, Rochester, NY 14627-0171, USA
[4] Institue for Astronomy, Swiss Federal Institute of Technology (ETH), CH-8093 Zurich, Switzerland
Received 2009 July 5; accepted 2010 March 22; published 2010 May 19

ABSTRACT

We present direct imaging observations at wavelengths of 3.3, 3.8 (L' band), and 4.8 (M band) μm, for the planetary system surrounding HR 8799. All three planets are detected at L' . The c and d components are detected at 3.3 μm, and upper limits are derived from the M-band observations. These observations provide useful constraints on warm giant planet atmospheres. We discuss the current age constraints on the HR 8799 system and show that several potential co-eval objects can be excluded from being co-moving with the star. Comparison of the photometry is made to models for giant planet atmospheres. Models that include non-equilibrium chemistry provide a reasonable match to the colors of c and d. From the observed colors in the thermal infrared, we estimate $T_{\rm eff} < 960$ K for b and $T_{\rm eff} = 1300$ and 1170 K for c and d, respectively. This provides an independent check on the effective temperatures and thus masses of the objects from the Marois et al. results.

Key words: instrumentation: adaptive optics – planets and satellites: atmospheres

Online-only material: color figures

1. INTRODUCTION

Over the past decade, a number of techniques have dramatically expanded our understanding of the nature of exoplanets. Initial detection of systems via radial velocity variations has been followed up by studies of transits, astrometric confirmation, and gravitational microlensing. All of these approaches have been helpful in developing our picture of planetary system architectures and providing insight into formation.

The direct imaging of extrasolar planets is the latest technique to provide useful information, with detection, of objects; first, around low-mass objects (Chauvin et al. 2004), followed, more recently, by the detection of several planets around intermediate mass stars (Kalas et al. 2008; Marois et al. 2008; Lagrange et al. 2009).

Direct images of extrasolar planets not dominated by insolation have the potential to provide a wealth of information about the size, temperature, composition, and even formation history of these objects. The recently discovered planetary system around HR 8799 (Marois et al. 2008), with three massive planets at large orbital separations, may provide one of the most useful laboratories to constrain the spectral energy distribution (SED) of young giant planets.

HR 8799 is a young A5V star, thought to be approximately 30–160 Myr old (Marois et al. 2006). It is known to have a bright debris disk at large orbital radii (Williams & Andrews 2006) with approximately 0.1 $M_{\rm Earth}$ of material at 50 K. A tenuous inner disk is thought to exist as well (Chen et al. 2006). Taken together with the planets, this suggests a system with an inner dust disk truncated by the d component at 24 AU and an outer disk truncated by the b component beyond ~80 AU. Su et al. (2009) also find an outflow of small grains, likely caused by gravitational stirring from the planets. The star also has a number of other interesting properties, including X-ray emission (Hearty et al. 1999; Schröder & Schmitt 2007) and a deficiency in refractory metals in the stellar atmosphere (the λ Boo phenomenon; Gray & Kaye 1999; Gray et al. 2003). Multiple metallicity estimates are consistent it being metal-poor (Fe/H $\simeq -0.5$; Gray & Kaye 1999), but having solar abundance lighter elements, such as carbon and oxygen (Sadakane 2006; Gerbaldi et al. 2007).

The planets around HR 8799 are interesting, particularly in the context of planet formation alternatives. If the planets formed in situ, the core accretion hypothesis (Pollack et al. 1996) would require formation of 10 $M_{\rm Earth}$ cores at distances of 40 and 70 AU well before the dispersal of the gas. A disk fragmentation scenario (Boss 1997; Nero & Bjorkman 2009; Dodson-Robinson et al. 2009; Helled & Bodenheimer 2009) may be able to more naturally explain the massive planets and their location. A more detailed look at the planet's environment and their SEDs can provide clues to these alternatives.

Models of the SED for planets (Burrows et al. 1997; Baraffe et al. 2003) are used to estimate the temperature and mass of the objects. However, these models are currently only constrained by field brown dwarfs and objects such as 2M1207, whose formation history is uncertain (Lodato et al. 2005; Mamajek & Meyer 2007). Are giant planets formed in a circumstellar disk around a normal star different? Objects such as the planets around HR 8799, as well as the planets around Fomalhaut (Kalas et al. 2008) and β Pic (Lagrange et al. 2009) may provide our first opportunity to address this topic. With multi-wavelength constraints of the brightness of the planets, we can disentangle effects from clouds, composition, and vertical mixing that may affect the measurement of the temperature, and thus the mass of the planets. By comparison of observations with field objects and current models, we may be able to develop a better understanding of the physics leading to the SEDs of giant exoplanets.

The 3–5 μm region provides access to both the 3.4 μm CH_4 feature and the CO bandhead at 4.7 μm. Observations of this

* Observations reported here were obtained at the MMT Observatory, a joint facility of the University of Arizona and the Smithsonian Institution.

portion of the SEDs provide useful constraints on the relative amount of CO to CH_4 in the atmospheres of these planets. The relative absorption of these species, in the near-infrared, is used to define the transition in spectral type between the L and T sequence among field brown dwarfs.

Observations of brown dwarfs in this region (Leggett et al. 2007) indicate that their colors are best reproduced by models that have substantial vertical mixing between the hot lower layers and the cooler upper atmosphere. Comparison of HR 8799 planets to these objects will allow us to better understand how closely exoplanet atmospheres may mimic those of field brown dwarfs.

Constraining the SED of giant planets in this region may help guide future direct imaging planet searches. Both Jupiter (Gillett et al. 1969) and Gliese 229 B (Oppenheimer et al. 1995) have a broad peak in the flux at 4–5 μm, suggesting that this may be a robust feature of brown dwarfs and giant planets in the $T_{\rm eff}$ = 100–1000 K range. However, various models indicate different bands as being preferable (cf. Marley et al. 1996; Burrows et al. 1997). In order to understand whether searching in L' or M band is preferable, it would be helpful to understand giant planet colors over the expected temperature range of these objects.

In this paper, we present observations at 3.3, 3.8, and 4.8 μm of the planets orbiting HR 8799. In Section 2, we describe the MMTAO and Clio camera observations of the HR 8799 system. Section 3 details the data reduction and analysis. Section 4 describes the photometric and astrometric results. Section 5 analyzes the age estimates for HR 8799. Section 6 compares these results to theoretical models and observations of brown dwarfs in the field. Finally, in Sections 7 and 8 we discuss the interpretation of the results and summarize our conclusions.

2. OBSERVATIONS

HR 8799 was observed on 2008 November 21, 2009 January 8, and 2009 September 12, using the MMT deformable secondary-based adaptive optics system (Wildi et al. 2003; Brusa et al. 2004). Cirrus clouds intermittently affected the throughput of the observations on 2008 November 21 and 2009 September 12.

The Clio camera (Freed et al. 2004; Sivanandam et al. 2006), an optimized instrument for exoplanet detection (Hinz et al. 2006; Heinze et al. 2006) in this spectral region, was used for the observations. The camera has a high flux detector that allows high duty cycle observations in the L' - and M-band atmospheric windows. Combined with the low background provided by a deformable secondary (Lloyd-Hart 2000), the system is capable of sensitive observations in the thermal infrared.

The Clio observations use the Barr M band ($\lambda = 4.8\,\mu$m, $\Delta\lambda = 0.6\,\mu$m; Simons & Tokunaga 2002), rather than the more common Mauna Kea Observatory (MKO) M' passband ($\lambda = 4.68\,\mu$m, $\Delta\lambda = 0.22\,\mu$m). The Barr M-band filter is preferred for sensitive M-band observations that maximize the signal-to-noise ratio (S/N) for the expected SED of a cool object (Freed et al. 2004). At L' the MKO filter was used. The zeropoints used for these filters are 248 Jy and 154 Jy for L' and M, respectively (Tokunaga & Vacca 2005; Bessell & Brett 1988).

In addition to standard MKO L' and Barr M-band filters, we carried out observations with a filter which was centered at 3.3 μm with half-power points at 3.10 μm and 3.5 μm. This filter is well matched to the methane absorption located at 3.4 μm and lies in the short wavelength region of the L-band atmospheric window. However, it is not closely related to any standard photometric system in the L window. We refer to it in the rest of the paper as the 3.3 μm filter and list magnitudes for this filter with the notation [3.3]. The zeropoint adopted for this filter is 330 Jy, obtained by interpolating between the L'- and K-band photometric zeropoint.

Clio observations are obtained by acquiring individual integrations of the detector with frame times set to avoid saturation by the background emission, typically 0.2 s for M band and 1.5 s for L' band. These individual exposures are accumulated into cubes of data with approximately 15–20 s total integration. Typically, five exposures are obtained before nodding the telescope in elevation. This results in the star being moved approximately every minute from one side of the detector to the other to provide periodic measurements of the sky background, as well as detector variations. Each nod pair provides a complete set of data with ten independent measurements of the field around HR 8799.

A significant source of noise in the images is static or slowly changing speckles. Their effect is minimized with the technique of angular differential imaging (e.g., Marois et al. 2006; Hinz et al. 2006). During the observations, the instrument derotator is not operated. This has the effect of causing the sky coordinates to slowly rotate relative to the detector coordinates. Since the static speckles stay fixed with respect to the telescope, we can remove them in the final image processing without affecting the flux from an off-axis companion.

Observations were taken in both L' and M band on 2008 November 21. Approximately 70° of rotation was obtained at L' and 30° at M band (see Table 1). For L'-band observations, 30 frames were rejected due to image jitter while observing near transit. The final image (see Figure 1) uses approximately 90 minutes of data. The M-band observations were taken just after this, as intermittent cirrus clouds began to form. Consequently, although approximately 170 minutes of integration was acquired, only 84 minutes of total integration (210 total frames) were used, after rejecting those images which showed stellar fluxes less than approximately 60% of the "clear" images.

A first set of 3.3 μm observations was taken on 2009 January 9, which required observing the star well after it had transited the meridian. This resulted in only a small amount of sky rotation for these observations. Consequently, for the 3.3 μm observations, we observed a standard star for use in point-spread function (PSF) subtraction. A total of 48 minutes of integration was obtained in the 3.3 μm filter.

A second set of 3.3 μm observations was taken on 2009 September 12. A total of 113 minutes of integration was obtained, with approximately 30° of rotation during the observations. Light clouds were present throughout the observations.

As can be seen in Figure 1, slowly changing speckles have different levels of importance for the three observed wavelengths. At 3.3 and 3.8 μm , the noise in the residual subtraction begin to degrade the detectability inside approximately 1″. However, for 4.8 μm observations, the brighter sky background and more stable PSF at longer wavelengths result in the images being sky-background limited even for the closest planet separation.

3. DATA REDUCTION AND ANALYSIS

The set of data was reduced with a custom-developed pipeline using the Perl Data Language (PDL[5]). A cube of frames for each observation is co-added to obtain individual images of 15.3, 14.6, and 24.0 s for the 3.3 μm, L' -, and M-band observations, respectively. Each image is subtracted from its pair in the

[5] http://pdl.perl.org

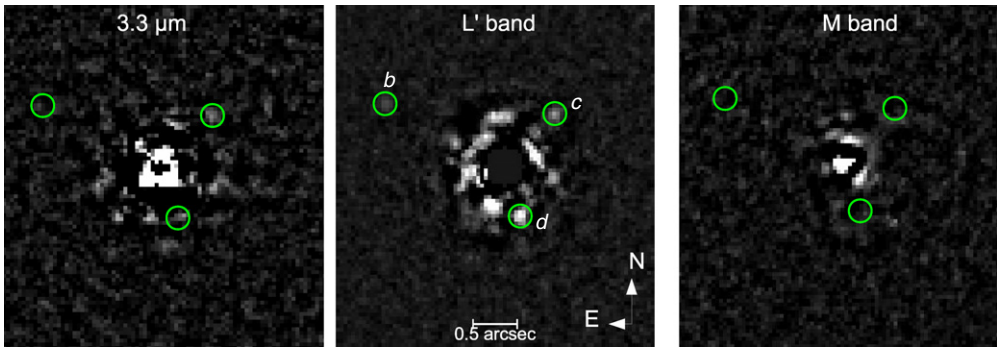

Figure 1. Images at 3.3 μm, L'(3.8 μm), and M (4.8 μm) of HR 8799. All three components are detected at L' (center). At 3.3 μm (left), only c and d are detectable. At M band (right), none of the planets are detectable above the sky background noise. The circles identifying the locations of the planets in each image are the approximate size of the photometric aperture used.

(A color version of this figure is available in the online journal.)

Table 1
Log of Data Acquisition for Clio Observations of HR 8799

Date	Total Integration (s)	Filter	Total Rotation (deg)
2008 Nov 21	5694	L'	72.0
2008 Nov 21	9600	Barr M	31.8
2009 Jan 9	2907	3.3 μm	5.3
2009 Sep 12	6780	3.3 μm	30.2

Table 2
Adopted Photometric Values for HR 8799

Band	Stellar Magnitude	Zeropoint (Jy)
3.3 μm	5.23	330
L'	5.22	235
M	5.21	154

other nod position to create two sky-subtracted images of the star. To eliminate the effect of slightly different gains among the four different channels, a blank portion of the detector is used to measure the average flux in each channel. This value is subtracted from all pixels corresponding to the appropriate channel. Finally, a bad pixel rejection routine is carried out which looks at the detector response for two successive nods to identify pixels which vary by more than 3 times the standard deviation. The values for these pixels are replaced by an average of their neighbors. The images are then shifted by measuring the centroid of the star and rotated by the parallactic angle of the observations to create a final image of the star with north up and east to the left in the image. A median PSF image is created by median combining all of the images without rotation. By subtracting this median PSF from all of the images prior to rotation, the majority of the diffraction and static aberration-induced scattered light can be removed from the final, combined image.

The measurements of the brightnesses of the planets are calculated relative to the measured flux from HR 8799 itself. Since the star is saturated in the L' and 3.3 μm images, images taken with neutral density filters or shorter exposures were obtained to measure the flux. The photometry is scaled from the Two Micron All Sky Survey (2MASS) K_s-band flux of HR 8799, using the expected K–L' and K–M colors for HR 8799's spectral type (Marois et al. 2008; Cox 2000); see Table 2.

The scale of the Clio pixels has been measured to be $0\farcs04857 \pm 0\farcs00003$ pixel^{-1}, using periodic observations of binary stars (Heinze 2007). The orientation of the detector relative to the sky is also calibrated with these measurements. North on the detector is $92\fdg27 \pm 0\fdg2$ counterclockwise from the top of the array.

4. OBSERVATIONAL RESULTS

To calculate the flux of the planets, apertures of size $0\farcs25$ were placed at the approximate locations of the sources. The images of the stars were measured with the same aperture to account for aperture-dependent effects. To estimate the errors in these measurements, each data set was split in half. For each half of the data set, a measurement of the image in each nod position was carried out, resulting in four independent measurements. The apparent magnitude and standard error in the mean for each set are reported in Table 3. For M band and some of the 3.3 μm data, the planets are not detected. For these data, 3σ upper limits are derived by measuring variations in flux with the same size aperture, at the same radial separation as the planet in an azimuthal arc around the star. We note that, typically, we conservatively quote 5σ–7σ limits for detection with Clio observations. However, for these observations, where we know the exact location of the planet, 3σ limits are more realistic estimates of our uncertainty in the flux contribution.

For comparison with models and other photometry, we adopt a distance of 39.4 pc to HR 8799 (van Leeuwen 2007). The photometric measurements of planets b, c, and d are reported in Table 3. We tabulate absolute and apparent magnitudes, as well as the "absolute" spectral flux density in millijanskys, or the flux at a distance of 10 pc. This is useful for comparisons with model SEDs. The L'-band measurements are consistent with Marois et al. (2008), within our photometric uncertainty.

The initial observations at [3.3] detected c but did not detect the other two components. Follow-up observations in 2009 September confirmed the detection of c and also detected d. We report the photometry for 3.3 μm from the 2009 September, as it is more sensitive than the 2009 January data, with better PSF subtraction. For the 2009 September data, there is a marginal source at the location of b. However, it is below the significance level of the image. We thus adopt the limiting magnitude for the image as the upper limit for b at 3.3 μm.

The astrometric measurements are calculated with a "center-of-light" algorithm within the photometric aperture. The same procedure of dividing up the data into four independent sets is used to calculate the astrometric uncertainty. These uncertainties are consistent with the astrometric measurement errors expected due to the PSF width of these observations and their low S/N

Table 3
Photometric Results

System	Band	*b*	*c*	*d*
Apparent Vega Magnitude	3.3 μm[a]	>17.8	15.63 ± 0.3	15.53 ± 0.3
	L'[b]	15.81 ± 0.23	14.99 ± 0.12	14.39 ± 0.19
	M[c]	>14.7	>14.7	>14.7
Absolute Vega Magnitude	$M_{3.3}$	>14.82	12.65 ± 0.3	12.55 ± 0.3
	$M_{L'}$	12.83 ± 0.23	12.01 ± 0.12	11.41 ± 0.3
	M_M	>11.72	>11.72	>11.72
Flux at 10 pc	$F_{3.3}$ (mJy)	<0.39	2.87 ± 0.86	3.15±.95
	$F_{L'}$ (mJy)	1.73 ± 0.41	3.69 ± 0.44	6.41 ± 1.9
	F_M (mJy)	<3.3	<3.3	<3.3

Notes.
[a] Custom filter with zeropoint listed in Table 2.
[b] MKO photometric system (Tokunaga & Vacca 2005).
[c] Bessell and Brett photometric system (Bessell & Brett 1988).

Table 4
Astrometric Results for Companions to HR 8799

Date	Band	HR 8799 *b* E [″], N [″][a]	HR 8799 *c* E[″], N[″][a]	HR 8799 *d* E[″], N[″][a]
2008 Nov 21	L'	1.542 ± 0.01, 0.780 ± 0.014	−0.631 ± 0.015, 0.″671 ± 0.02	−0.215 ± 0.021, −0.644 ± 0.013
2009 Jan 9	3.3 μm	...	−0.612 ± 0.03, 0.″665 ± 0.03	...
2009 Sep 12	3.3 μm	...	−0.625 ± 0.02, 0.″725 ± 0.02	−0.282 ± 0.03, −0.590 ± 0.03

Note. [a] Offset from HR 8799.

(Lindegren 1978). Astrometric results for the observations are summarized in Table 4. The L' position of planets *b* and *c* are consistent with the Marois results, differing by 24 and 44 mas, respectively. The L' *d* position is displaced by 62 mas from the reported Marois position. Since the orbital motion expected for this object is only 7 mas over the two month time span between the two observations, the discrepancy of *d* is not easy to explain. It is possible that the positional difference is an indication of contamination of the flux by a residual speckle in the final image. The [3.3] position of *d* is also 66 mas from the Marois position, but since the observations were taken a year after those results, the difference is similar to the expected orbital motion. This effect can be seen in Figure 1, where the position of *d* in the [3.3] image is significantly shifted relative to the L' image.

5. ON THE AGE AND STELLAR MULTIPLICITY OF HR 8799

Understanding the age of the HR 8799 system is important for interpreting the SEDs of the planetary companions and assessing their stability. For example, Fabrycky & Murray-Clay (2010) and Reidemeister et al. (2009) analyze the stability of this system, for which one of the crucial parameters is its age. Marois et al. (2008) assign an age for HR 8799 of 60^{+100}_{-30} (30–160) Myr, and previously Moór et al. (2006) estimated an age of 20–150 Myr based on assigning HR 8799 membership to the Local Association. Marois et al. (2008) based the age on careful consideration of four diagnostics: (1) the star's space motion and possible association with HD 984 and HD 21318, as well as the Columba and Carina Associations; (2) its position in a color–magnitude diagram; (3) the typical age of λ Boo and γ Dor variables; and (4) the large mass of its debris disk. Of these, only the star's position on a color–magnitude diagram provides a quantitative constraint. Here, we explore whether association of HR 8799 with any additional companions or moving groups can be used to further refine its age estimate.

5.1. On the Association with HD 984 and HD 21318

Marois et al. (2008) calculate a space motion for HR 8799 of $UVW = (-11.9, -21.0, -6.8)\,\mathrm{km\,s^{-1}}$ and suggest that it is similar to other young stellar groups in the solar neighborhood (e.g., Columba, Carina, etc.) as well as two neighboring stars: HD 984 and HD 21318 to which they assign ages of ∼30 and ∼100 Myr, respectively. We investigate the space motion of HR 8799 here and discuss Columba and Carina groups in the following subsection. Using the revised Hipparcos astrometry van Leeuwen (2007) and the radial velocity from the compiled RV catalog of Gontcharov (2006), we estimate the velocity of HR 8799 to be $UVW = (-12.2, -21.2, -7.2) \pm (0.6, 0.8, 1.2)\,\mathrm{km\,s^{-1}}$. Using astrometry from van Leeuwen (2007) and radial velocities from Holmberg et al. (2007), we independently verify that the stars HD 984 and HD 21318 have space motions within $3.6 \pm 2.0\,\mathrm{km\,s^{-1}}$ and $1.0 \pm 1.8\,\mathrm{km\,s^{-1}}$ of HR 8799, respectively. The HD 984 and HD 21318 are separated by 26 and 19 pc from HR 8799, respectively. We simulated the orbits of HR 8799 and these two stars using the epicyclic approximation, adopting the Oort constants from Feast & Whitelock (1997) and the LSR velocity from Dehnen (1998), and the local disk density from van Leeuwen (2007). We find that HD 8799 and HD 984 were not significantly closer to one another within the past 100 Myr (although some ∼0.02 pc closer ∼0.5 Myr ago) and were probably separated by ∼80 pc ∼30 Myr ago. We find that HR 8799 and HD 21318 would have been separated by ∼140 pc ∼100 Myr ago, with the nearest pass being ∼13 pc away ∼11 Myr ago. While $\sim 1\,\mathrm{km\,s^{-1}}$ uncertainties in the velocities can lead to large uncertainties in the distant past ($\sim 1\,\mathrm{pc\,Myr^{-1}}$), any genetic tie between HR 8799 and HD 984 and HD 21318 would seem tenuous at best.

5.2. On the Association with Columba and Carina

Is HR 8799 related to the putative Columba or Carina groups? We adopt our revised space motion for HR 8799

and the parameters of the velocity and position centroid for Columba and Carina from Torres et al. (2008) and ran the stars through our epicyclic orbit code. HR 8799 is currently 98 pc from the centroid of Columba, as defined by Torres et al. (2008), and its closest approach to the group within the past 160 Myr was a pass ∼27 Myr ago ($\Delta \simeq 58$ pc), which seems too distant to be a plausible candidate for ejection/evaporation. Similarly, HR 8799 is currently ∼116 pc distant from the centroid for Carina, and its closest approach within the past 160 Myr was ∼37 Myr ago ($\Delta \simeq 45$ pc)—also relatively distant for a plausible association. We find that the centroids of Columba and Carina were closest to one another ∼18 Myr ago with a separation of ∼24 pc. While the putative groups themselves are very large (tens to >100 pc), it is more likely that they constitute "complexes" with a wide range of ages, making membership—even if likely—not useful for assigning ages.

5.3. On the Candidate Common Proper Motion Stars Found by Close & Males (2010)

Close & Males (2010) found no evidence for bound companions using archival Gemini and *HST*/NICMOS images. They also identified a few candidate common proper motion stars within a degree using NOMAD/USNO-B1.0 astrometry (Monet et al. 2003; Zacharias et al. 2005), however, none are particularly strong candidates for being associated with HR 8799. Despite the similarity of their proper motions to that of HR 8799, the two top co-moving companion candidates identified by Close & Males (2010) can be ruled out through further consideration of their photometry. NOMAD 1115-0634383 (J2000; 23 10 22.93 + 21 34 20.7) is 48′ distant from HR 8799 and is very red. We find that the 2MASS JHK photometry for this object (J–$H = 0.58 \pm 0.04$ mag, H–$K_s = 0.22 \pm 0.04$ mag) is consistent with an unreddened M2V (±1 subtype). This corresponds well with the B–V estimated by Close & Males (2010) (B–$V \simeq 1.61$; inferred from NOMAD photographic magnitudes) and with a V–K_s color (≃4.5 mag) that we calculate using USNO-A2.0 B & R photometry[6] and 2MASS K_s. However, if the star is an unreddened M1V-M3V dwarf at distance = 39 pc ($M_V \simeq 13.9$ mag), it is approximately 2–4 mag below the main sequence and hence could not be related to HR 8799. Similarly, the second best candidate companion NOMAD 1108-0634609 (TYC 1717-1120-1) can be rejected on similar grounds. The V–K_s color (1.87 ± 0.04; Cutri et al. 2003; Droege et al. 2007) is consistent with an unreddened G8V (±1 subtype). At a distance of 39 pc, the observed V magnitude ($V = 10.50$; Droege et al. 2007) would correspond to $M_V = 7.52$, which is ∼2 mag fainter than typical G8V dwarfs. The colors of both candidates are also far too red to correspond to unreddened young (∼10^7–10^8 yr) degenerate stars (see, e.g., Kalirai et al. 2003). Reddening is unlikely to be responsible for the brightness deficits of these two objects: reddening is negligible within 75 pc of the Sun (e.g., Leroy 1993) and HR 8799 itself has negligible reddening (Zerbi et al. 1999). We conclude that both the two strongest NOMAD candidates identified by Close & Males (2010) are probably background field stars, unassociated with HR 8799.

5.4. Search for Co-moving Stars Within 10° Radius

Some of the famous young nearby stars in the solar vicinity have been found to belong to stellar associations which help in their age-dating (e.g., TW Hya, AB Dor), mostly through combining X-ray and astrometry data to search for active, co-moving stars (Zuckerman & Song 2004). This motivated us to search for evidence of a group in the vicinity of HR 8799 similar to other studies above. At present, we focus on X-ray/astrometric selection since astrometric selection alone is rather daunting and produces a substantial chance of false positives (e.g., Close & Males 2010). We searched a 10° (∼10 pc) radius around HR 8799 for signs of co-moving low-mass stars with a cross-referenced list of X-ray-emitting stars (Voges et al. 1999, 2000) in the *Tycho-2* and UCAC2 astrometric catalogs (Hog et al. 2000; Zacharias et al. 2003). As the three-dimensional velocity of HR 8799 is well defined, we tested whether the motions of these stars were consistent with motion toward HR 8799's convergent point (α, δ = 99.°5 ± 2.°8, −31.°1 ± 1.°8). The most interesting system identified was the dMe star [K92] 94 (= 2MASS J23081213+2126198)[7] situated 1235″ away from HR 8799. The star was originally discovered due to modest Hα emission by Kun (1992) and later classified as M0V without Hα emission by Martin & Kun (1996). However, if placed at 39 pc, its absolute K magnitude ($M_K \simeq 8.1$; based on 2MASS K_s photometry) would be ∼3 mag fainter than a typical young disk M0V star ($M_K \simeq 4.8$; Leggett 1992). Combined with the fact that its tangential motion differs from that of HR 8799 by ∼4 km s^{-1}, it seems unlikely that [K92] 94 is associated with HR 8799.

We therefore conclude that there still is no evidence for any co-moving stellar companions to HR 8799 which could help constrain its age. For the purpose of estimating planet masses, we thus use the same age estimate as Marois et al. (2008) of 60^{+100}_{-30} Myr.

6. COMPARISON TO GIANT PLANET MODELS AND BROWN DWARFS

The observational results above can be used to constrain the physical parameters for the planets around HR 8799. We have used two separate approaches: comparison with young, giant planet models in the literature and comparison with field brown dwarf photometry and spectra.

For the giant planet models, we can use the evolutionary cooling tracks of Burrows et al. (1997), hereafter B97, to estimate the size of the planets. The modeled radii of objects in the mass range of 5–20 $M_{\rm Jup}$ and an age range of 30–160 Myr vary from 1.15 to 1.29 $R_{\rm Jup}$. We adopt a radius of 1.22 $R_{\rm Jup}$ to estimate the flux density from the model SEDs. This size suggests that a gravity of log g = 4.0–4.6 is expected for these objects. We use models of log g = 4.5 for comparison with the observations.

Because of the small variations in radius versus age and mass, the key observable to constrain is the effective temperature of the objects. Depending on the age of the system, the effective temperatures will correspond to different mass estimates.

6.1. Giant Planet Models

Models of brown dwarf and giant planet atmospheres have been carried out with increasing levels of detail over the past decade. Non-gray atmospheres have been computed by Burrows et al. (1997, 2003) and by Baraffe et al. (2003) that cover

[6] http://www.aerith.net/astro/color_conversion.html

[7] The originally published position from Kun (1992) is apparently off by ∼30″. We correctly matched the 2MASS source to the star using the finder chart in Figure 8 of Kun (1998) and SkyView (http://skyview.gsfc.nasa.gov/).

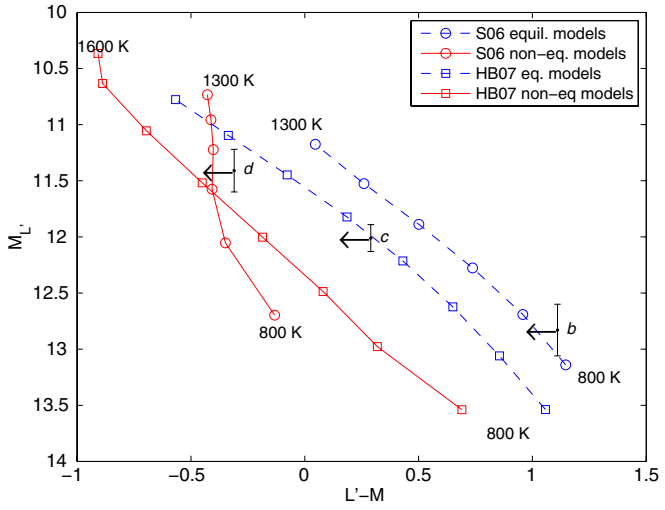

Figure 2. Color–Magnitude relation for models compared to observed photometry. Model colors are shown from Hubeny & Burrows (2007) and Saumon et al. (2006). The temperature range spans 800–1600 K for the HB07 models and 800–1300 K for the S06 models. The models use $K_{zz} = 10^4$ cm^2 s^{-1}, log $g = 4.5$, and a cloudy atmosphere model. A chemical reaction rate corresponding to the "slow" rate is used for the HB07 models, and the "fast2" rate is used for the S06 models.

(A color version of this figure is available in the online journal.)

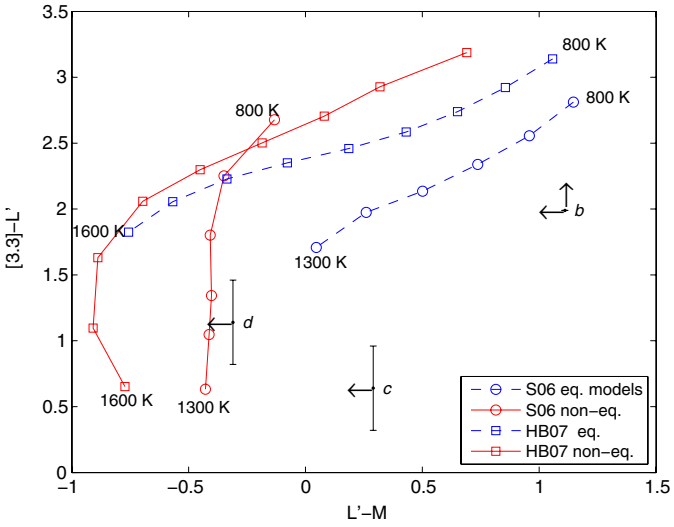

Figure 3. Color–Color plot for L'-M vs. [3.3]–L'. Models from Hubeny & Burrows (2007) and Saumon et al. (2006) are shown. The same parameters are used as in Figure 2.

(A color version of this figure is available in the online journal.)

this temperature range. The effects of both clouds and non-equilibrium chemistry have been studied by Saumon et al. (2006) and Hubeny & Burrows (2007). Hubeny & Burrows (2007) have developed a grid of models using various diffusion coefficients, reaction rates for CO → CH_4 and gravities. They find that the M-band flux, in particular, is affected for $T_{\rm eff} \sim 1000$ K, exactly the range for the three HR 8799 planets. Saumon & Marley (2008, and references therein) have developed models that incorporate vertical mixing (Saumon et al. 2006; Leggett et al. 2007) and increased metallicity (Fortney et al. 2008) to match spectra of brown dwarfs and predict the SEDs of giant planets. We compare the observations above to families of models by Saumon et al. (2006, hereafter S06) and Hubeny & Burrows (2007, hereafter HB07) that include these effects.

We plot a color versus magnitude at L' and M in Figure 2 to compare the observations with the models. The M-band limits are the 3σ limits listed in Table 3. The data are compared to both models that are in chemical equilibrium and models which incorporate non-equilibrium chemistry. While b could be fit by any of the model sets, the location of c is inconsistent with the equilibrium S06 models and that of d is inconsistent with both sets of equilibrium models. For both the HB07 models and the S06 models, the non-equilibrium sequence uses an eddy diffusion coefficient (K_{zz}) of 10^4 cm^2 s^{-1}. The HB07 models shown use the "slow" reaction for the CO → CH_4 chemical reaction described in Hubeny & Burrows (2007). The S06 models use an equivalent rate to the "fast2" rate described in HB07 (D. Saumon 2010, private communication). The models incorporate clouds and are calculated for log $g = 4.5$. The temperatures for each sequence are in 100 K increments, from 800 K to 1600 K for the HB07 models and 800 to 1300 for the S06 models. The colors suggest that, as with brown dwarfs (Leggett et al. 2007), the HR 8799 objects are best fit by models which incorporate vertical mixing into the atmospheres.

Figure 3 shows a color–color plot for the object and models, using L'–M versus [3.3]–L. The models shown are the same as for Figure 2. Due to its faintness, the limits on b are consistent with any of the models. The [3.3]–L' color of c and d is bluer than predicted by the equilibrium models over the range of temperatures considered. The HB07 non-equilibrium models are only consistent with the [3.3]–L' color for effective temperatures above 1500 K, for c, and 1430 K, for d. The S06 non-equilibrium models are well matched to colors, for c, which correspond to 1200–1350 K and, for d, 1050–1250 K. For b, the effective temperature estimated from the S06 model colors is below 950 K. In general, the S06 models indicate cooler temperatures by ∼300 K for all three planets, compared to the HB07 models.

Model fits to the [3.3]–L' color can be used to estimate the effective temperatures of the planets. These fits are shown in Figure 4. The HB07 models result in $T_{\rm eff} < 1310$ K for b, and $T_{\rm eff} = 1620$ and 1490 K for c and d. For the S06 models, the corresponding results are <940 K for b, and 1300 and 1170 K for c and d, respectively.

The model fits to the colors do not constrain the overall flux. If a size of 1.2 $R_{\rm Jup}$ is used to estimate the flux, consistent with expected size of these objects from the B97 models, the results are significantly brighter than the observed photometry at L'. To match the observed flux at the best-fit temperatures, the planets would need to be smaller than expected from the B97 models. For the HB07 models, planets c and d would need to have radii which are 44% and 63% of their expected size of 1.2 $R_{\rm Jup}$. For the S06 models, the radii would need to be 56% and 84% as big.

Figure 5 again shows the SEDs of the HB07 and S06 models compared to the HR 8799 photometry, but now matched to the absolute magnitude at L' (M'_L). For each planet, a model temperature is selected that best fits the value of M'_L, using an assumed radius of 1.22 $R_{\rm Jup}$ for the planets. The effective temperature and model parameters corresponding to the fit for each plot is inset in the graph. For the non-equilibrium SEDs, the average modeled flux in each passband is plotted as a horizontal line spanning the passband. The difference in the best-fit SEDs between the HB07 and S06 models suggests that the details of how the vertical mixing is modeled is important for accurate estimates of colors, especially in the 3.3 μm portion of the spectrum.

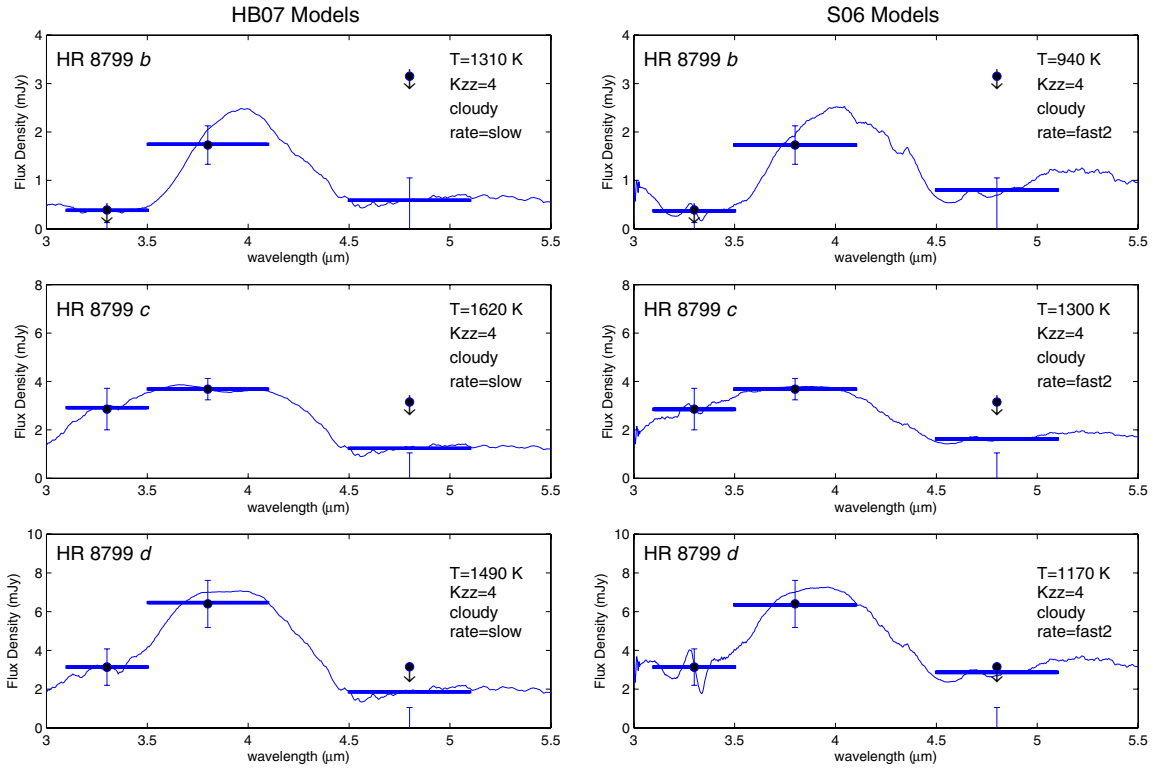

Figure 4. Comparison of HR 8799 photometry to models by Hubeny & Burrows (2007) and Saumon et al. (2006) for *b* (top), *c* (middle), and *d* (bottom). For each planet, models are shown that best match the [3.3]–L' color. The overall flux is allowed to vary to fit both the [3.3] and L' photometric points. The band-integrated flux density of the models is shown as horizontal lines for the observed passbands.

(A color version of this figure is available in the online journal.)

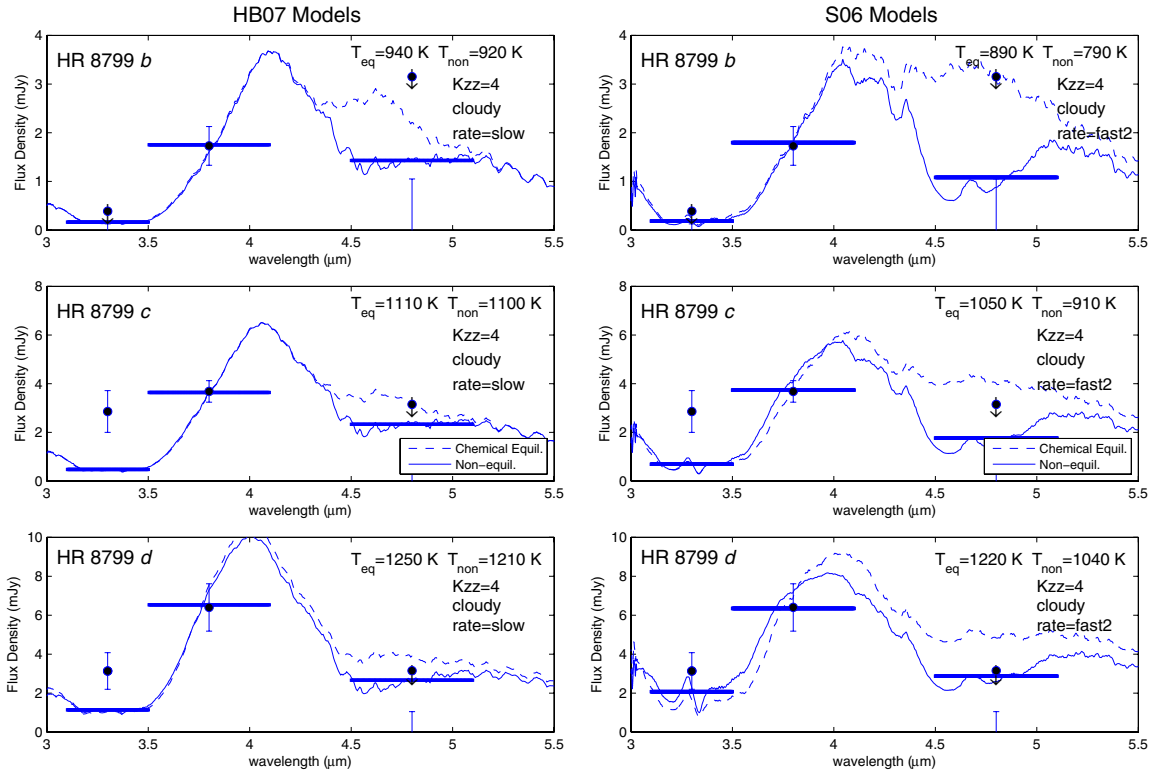

Figure 5. Comparison of HR 8799 photometry to models by Hubeny & Burrows (2007) and Saumon et al. (2006) for *b* (top), *c* (middle), and *d* (bottom). For each planet, models are shown that best match the L' -band photometry. The chemical equilibrium models appear to overpredict the *M*-band flux, while non-equilibrium models are consistent with the 3σ upper limits. The band-integrated flux density of the non-equilibrium models is shown as horizontal lines for the observed passbands.

(A color version of this figure is available in the online journal.)

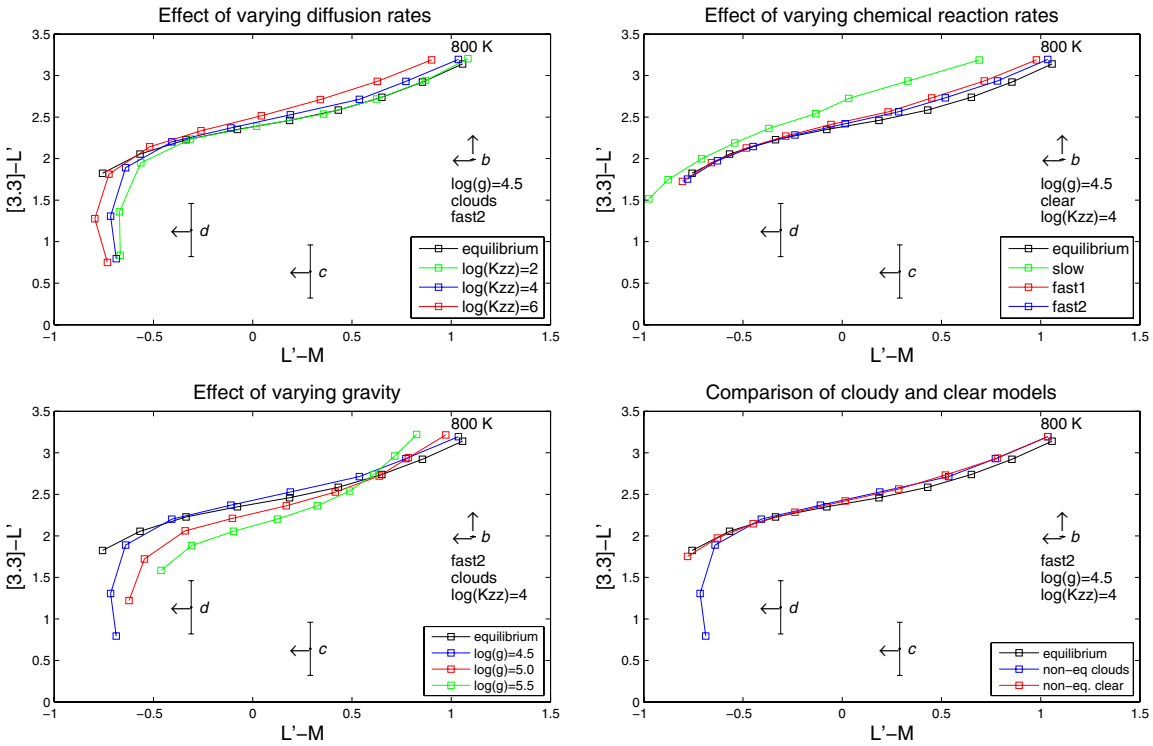

Figure 6. Color–Color plots using the Hubeny & Burrows (2007) models. The upper left compares different diffusion rates. The right compares different reaction rates. The lower left compares varying gravity, while the lower right compares cloudy and clear models. The models are unable to reproduce the [3.3]–L' colors unless temperatures above $T_{\rm eff} = 1400$ K are used.

(A color version of this figure is available in the online journal.)

Different diffusion rates, reaction rates, and gravities, as well as a comparison of cloudy and clear models, were explored for the HB07 models. These comparisons are shown in Figure 6. Only cloudy models are available for the various reaction rates tried, while the varying diffusion rates are only calculated for clear models. While this leads to an imperfect comparison, the general trend for each parameter can be seen. Cloudy models can reproduce the [3.3]–L'colors seen for c and d, but only for $T_{\rm eff} > 1400$ K. The other parameters do not significantly affect the [3.3]–L' colors.

6.2. Comparison to Brown Dwarf Spectra

Another useful comparison to the observational results can be found in the colors of brown dwarfs in the field. Although field brown dwarfs of similar temperature to the HR 8799 are likely more massive, due to their being older, they might still be expected to provide a good approximation of the expected SEDs of these objects.

Although the [3.3]–L' colors are blue relative to most model SEDs, similar colors are seen in spectra for brown dwarfs at these effective temperatures. In addition, the observed [3.3]–L' color changes significantly for spectral types in the L9 to T3 range, confirming that this region of the spectrum is useful for constraining the physical parameters of brown dwarf and giant planet atmospheres in this temperature range. For example, Leggett et al. (2008) analyze HN Peg B in detail and Stephens et al. (2009) present infrared spectra of a large sample of brown dwarfs, including 3–4 μm spectra of a subset of the objects. The objects SDSS 1207+02, SDSS 0758+32, HN Peg B, and 2M 0559-14 with spectral types of T0, T2, T3, and T4.5 have [3.3]–L' colors of approximately 0.75, 1.2, 1.9, and 2.5, respectively. HR 8799 c and d have a [3.3]–L' color of 0.63 and 1.16, respectively. This suggests that the [3.3]–L' colors of c and d are consistent with a T0 $\pm$ 1 and T2 $\pm$ 1 dwarf, respectively. From the temperature scale of Golimowski et al. (2004) as revised by Stephens et al. (2009), this would indicate $T_{\rm eff} = 1200$–1300 K, for these objects, consistent with the S06 models. b has a [3.3]–L' color of >1.9 constraining its spectral type to be later than T2, or $T_{\rm eff} < 1200$ K. Of course, the Stephens et al. (2009) $T_{\rm eff}$ versus spectral type relation shows scatter of $\sim$100 K about a given spectral type, suggesting that caution should be taken in comparing these results.

Finally, we note that the H–[4.5] color–temperature relation developed by Warren et al. (2007) can be used to constrain the temperature of these objects, assuming that they have similar emergent spectra to field brown dwarfs. Leggett et al. (2007) derive a constant [4.5]–$M' = -0.3$ color correction for objects in this temperature range. From the Marois et al. (2008) H-band photometry, we calculate an H–[4.5] color of less than 2.47, 1.63, and 1.56 for b, c, and d, respectively. Using the Warren scale, we derive temperature greater than 900, 1100, and 1150 K for the objects, consistent with the color-derived estimates from the S06 models.

7. DISCUSSION

The key feature of the 3–5 μm results is the blue color of the photometry, compared to equilibrium models. While the L'–M colors can be matched with the HB07 models, the [3.3]–L' model colors are too red unless effective temperatures of >1400 K are used. Vertical mixing can explain both the M-band and 3.3 μm observations in the S06 models. The difference between these similar model families suggests that the details of how the non-equilibrium chemistry is modeled appears to be an important factor in the resulting SED. Janson et al. (2010)

reach a similar conclusion from their analysis of *c*'s spectrum in the *L* band.

Even the S06 models have a discrepancy between the effective temperature derived from the [3.3]–L' color and the best fit according to the L' photometry, with the $T_{\rm eff}$ predicted to be ∼100–400 K lower from the L' photometry compared to the color-derived temperature. The correspondence of the color-derived temperatures from S06 models with those of field brown dwarfs suggest that the model temperatures are reasonable. Based on the effective temperatures, the derived masses from the cooling models of Baraffe et al. (2003) are $12 \pm 2\ M_{\rm Jup}$ for *c* and $11 \pm 2\ M_{\rm Jup}$ for *d* for an assumed age of 60 Myr. The temperature limit on *b* results in a mass limit of $<9\ M_{\rm Jup}$. These mass estimates are consistent with the estimates from Marois et al. (2008).

The large age range for the HR 8799 system (30–160 Myr) increases the uncertainty in the estimated mass of these objects. This error term is larger than that from the photometry, resulting in a mass range of $\sim \pm 3\ M_{\rm Jup}$ for the objects. Combined with the photometric uncertainty, this indicates a mass of $12 \pm 4\ M_{\rm Jup}$ for *c*, 11 ± 4 for *d*, and an upper limit on *b* of $<12\ M_{\rm Jup}$.

The dimness of *c* and *d*, given the color-derived temperatures, is problematic for any evolutionary model of a giant planet. Even a very old object will not be small enough to match the L' apparent magnitudes. The best fits to $T_{\rm eff}$ of *c* and *d* result in radii for the objects of 0.7 and 1.0 $R_{\rm Jup}$, respectively. Given the young age of HR 8799, a possible explanation of this discrepancy is that dust extinction of approximately 1.3 and 0.4 mag at L' is reducing the observed flux for *c* and *d*, respectively. Since HR 8799 is relatively nearby and shows no sign of foreground extinction, this dust obscuration would need to be intrinsic to the objects themselves.

Alternatively, lower gravity, metallicity, details of the chemical abundance versus height, or even incorrect opacity estimates for methane may be affecting the colors. Models with $\log g = 4$ for the S06 were also compared to the observations, but were not different from the $\log g = 4.5$ models shown. However, it is possible that gravity, combined with effects not properly captured in these models (such as metallicity or details of the chemical abundance variation versus height), may be affecting the colors for these objects in a more significant way than for field brown dwarfs. Typical field brown dwarfs have median ages of ∼3 Gyr (Dahn et al. 2002). Hence, the typical gravity of a $T_{\rm eff} = 1000$ K object in the field is $\log g = 5.0$, while these objects are expected to have $\log g = 4.3$. If the vertical mixing is similar for both the field brown dwarfs and the planets, it is reasonable to expect that the stronger than expected CO absorption and the weaker than expected CH_4 absorption are an effect of the lower gravity.

Interestingly, the NIR colors of these objects, as well as 2M1207b, are redder than field brown dwarfs of the same brightness (Marois et al. 2008). The NIR color difference could well be explained by their youth, and thus their lower gravity. Indeed, the young field L dwarf 2M0141-4633, found by Kirkpatrick et al. (2006), has nearly identical NIR photometry to *c* and *d* and is discrepant with other field L dwarfs. The estimated mass of 6–25 $M_{\rm Jup}$ for this object indicates that it should have similar gravity to the HR 8799 planets. This suggests that the red NIR colors are a low gravity effect. Kirkpatrick et al. attribute the red colors to lower collision-induced absorption of H_2, which primarily suppresses the *K* band. At lower gravities the H_2 CIA is reduced, causing the redder *H*–*K* color. Thus, while the color trend is opposite in the thermal IR, it appears that both effects might be explained by the youth, and low gravity, of the objects.

While in principle, the balance between CO and CH_4 in these atmospheres is governed by Le Chatelier's principle (Burrows et al. 2001), the details of how the vertical mixing occurs appears to be important in predicting the emergent spectra. An additional effect may be the metallicity of the atmospheres (Fortney et al. 2008). In higher metallicity objects, the formation of CO is expected to be enhanced, since more oxygen is available relative to hydrogen, compared to lower metallicity atmospheres. This suggests that giant planet atmospheres would be blue in the 3–5 μm region for more metal-rich objects.

Although HR 8799 is a metal-poor star, detailed observations (Gray & Kaye 1999) indicate solar abundance for lighter elements (Sadakane 2006), a consequence of the λ Boo phenomenon. This suggests that models with solar metallicity are probably appropriate for interpreting the colors of the HR 8799 planets. The solar metallicity (or perhaps metal-poor if the λ Boo phenomenon is discounted) cannot explain the blue 3–5 μm colors. If the formation of the planets caused them to be significantly metal-enhanced relative to their stars, this may be able to explain their colors. Further observations may be able to disentangle the metallicity of these objects from the other parameters which govern their SEDs. At the same time, detailed models are needed to explore the potentially complex interplay between gravity, vertical mixing, and metallicity.

It is interesting to note that mass estimates, derived from model fits to the L' photometry, are not significantly different from color-derived estimates. For example, the non-equilibrium fits from the HB07 models, for an age of 60 Myr, result in mass estimates of 9, 10.5, and 11 $M_{\rm Jup}$ for *b*, *c*, and *d*, respectively. If we use the S06 models, the estimates are 7, 9, and 10 $M_{\rm Jup}$, respectively. The HB07 models are likely a better estimate of the effective temperature from the M'_L values, since these models treat the temperature profile in a self-consistent way with the vertical mixing, while the S06 models do not take this into account. The SEDs for these objects, as shown in Figure 5, indicate that the non-equilibrium ones are consistent with the L'–*M* colors, while being discrepant with the [3.3]–L' colors. Although the internal inconsistencies point toward a need for better models and further observations, the current results all indicate that the objects are massive ($>10\ M_{\rm Jup}$), providing a challenge to models for explaining the stability of the system (Fabrycky & Murray-Clay 2010; Reidemeister et al. 2009) as well as its formation.

8. SUMMARY

Measurements of HR 8799 in thermal IR have constrained the SED of these planets, helping to better understand their physical parameters. The L'–*M* and [3.3]–L' colors of the objects appears to be blue, relative to equilibrium models. Models which account for non-equilibrium chemistry of CO and CH_4 can account for this effect, but the details of the modeling lead to differing results, depending on the input assumptions. Improved modeling of these objects will help understand the source of this. Deeper 3.3 μm and *M*-band photometry will be helpful in constraining the SEDs of these interesting objects.

The effective temperatures of *b*, *c*, and *d* derived from the colors as predicted by the S06 models are <940, 1300, and 1170 K, indicating the objects are $<9\ M_{\rm Jup}$ for *b* and 12 and 11 $M_{\rm Jup}$ for *c* and *d* for an assumed age of 60 Myr. These estimates provide an independent constraint from the Marois

et al. (2008) results on the effective temperatures and masses of the companions to HR 8799. The results confirm the massive nature of this planetary system and highlight the need for more detailed models to fit the colors of these objects.

We are grateful to the staff of the MMT, especially Ricardo Ortiz and Tim Pickering, who were instrumental in obtaining the data. We thank the Hectospec queue observers for graciously allowing us to exchange time. We thank Faith Vilas and Peter Strittmatter for their assistance in enabling these observations. Thank you to Didier Saumon, Ivan Hubeny, Adam Burrows, and Jonathan Fortney for providing model spectra for comparison with the observations.

REFERENCES

Baraffe, I., Chabrier, G., Barman, T. S., Allard, F., & Hauschildt, P. H. 2003, A&A, 402, 701
Bessell, M. S., & Brett, J. M. 1988, PASP, 100, 1134
Boss, A. P. 1997, Science, 276, 1836
Brusa, G., Miller, D. L., Kenworthy, M. A., Fisher, D. L., & Riccardi, A. 2004, Proc. SPIE, 5490, 23
Burrows, A., Hubbard, W. B., Lunine, J. I., & Liebert, J. 2001, Rev. Mod. Phys., 73, 719
Burrows, A., Sudarsky, D., & Lunine, J. I. 2003, ApJ, 596, 587
Burrows, A., et al. 1997, ApJ, 491, 856
Chauvin, G., Lagrange, A.-M., Dumas, C., Zuckerman, B., Mouillet, D., Song, I., Beuzit, J.-L., & Lowrance, P. 2004, A&A, 425, L29
Chen, C. H., et al. 2006, ApJS, 166, 351
Close, L. M., & Males, J. R. 2010, ApJ, 709, 342
Cox, A. N. (ed.) 2000, Allen's Astrophysical Quantities (New York: AIP Press)
Cutri, R. M., et al. 2003, 2MASS All Sky Catalog of Point Sources, http://irsa.ipac.caltech.edu/applications/Gator/
Dahn, C. C., et al. 2002, AJ, 124, 1170
Dehnen, W. 1998, AJ, 115, 2384
Dodson-Robinson, S. E., Veras, D., Ford, E. B., & Beichman, C. A. 2009, ApJ, 707, 79
Droege, T. F., Richmond, M. W., & Sallman, M. 2007, VizieR Online Data Catalog, 2271, 0
Fabrycky, D. C., & Murray-Clay, R. A. 2010, ApJ, 710, 1408
Feast, M., & Whitelock, P. 1997, MNRAS, 291, 683
Fortney, J. J., Marley, M. S., Saumon, D., & Lodders, K. 2008, ApJ, 683, 1104
Freed, M., Hinz, P. M., Meyer, M. R., Milton, N. M., & Lloyd-Hart, M. 2004, Proc. SPIE, 5492, 1561
Gerbaldi, M., Faraggiana, R., & Caffau, E. 2007, A&A, 472, 241
Gillett, F. C., Low, F. J., & Stein, W. A. 1969, ApJ, 157, 925
Golimowski, D. A., et al. 2004, AJ, 127, 3516
Gontcharov, G. A. 2006, Astron. Astrophys. Trans., 25, 145
Gray, R. O., Corbally, C. J., Garrison, R. F., McFadden, M. T., & Robinson, P. E. 2003, AJ, 126, 2048
Gray, R. O., & Kaye, A. B. 1999, AJ, 118, 2993
Hearty, T., Magnani, L., Caillault, J.-P., Neuhäuser, R., Schmitt, J. H. M. M., & Stauffer, J. 1999, A&A, 341, 163
Heinze, A., Hinz, P., Sivanandam, S., Apai, D., & Meyer, M. 2006, Proc. SPIE, 6272, 121
Heinze, A. N. 2007, Ph.D. thesis, Univ. Arizona
Helled, R., & Bodenheimer, P. 2009, arXiv:0911.5003
Hinz, P. M., Heinze, A. N., Sivanandam, S., Miller, D. L., Kenworthy, M. A., Brusa, G., Freed, M., & Angel, J. R. P. 2006, ApJ, 653, 1486
Hog, E., et al. 2000, VizieR Online Data Catalog, 1259, 0
Holmberg, J., Nordström, B., & Andersen, J. 2007, A&A, 475, 519
Hubeny, I., & Burrows, A. 2007, ApJ, 669, 1248 (HB07)
Janson, M., Bergfors, C., Goto, M., Brandner, W., & Lafrenière, D. 2010, ApJ, 710, L35
Kalas, P., et al. 2008, Science, 322, 1345
Kalirai, J. S., Fahlman, G. G., Richer, H. B., & Ventura, P. 2003, AJ, 126, 1402
Kirkpatrick, J. D., Barman, T. S., Burgasser, A. J., McGovern, M. R., McLean, I. S., Tinney, C. G., & Lowrance, P. J. 2006, ApJ, 639, 1120
Kun, M. 1992, A&AS, 92, 875
Kun, M. 1998, ApJS, 115, 59
Lagrange, A., et al. 2009, A&A, 493, L21
Leggett, S. K. 1992, ApJS, 82, 351
Leggett, S. K., Saumon, D., Marley, M. S., Geballe, T. R., Golimowski, D. A., Stephens, D., & Fan, X. 2007, ApJ, 655, 1079
Leggett, S. K., et al. 2008, ApJ, 682, 1256
Leroy, J. L. 1993, A&A, 274, 203
Lindegren, L. 1978, in IAU Colloq. 48, Modern Astrometry, ed. F. V. Prochazka & R. H. Tucker (Cambridge: Cambridge Univ. Press), 197
Lloyd-Hart, M. 2000, PASP, 112, 264
Lodato, G., Delgado-Donate, E., & Clarke, C. J. 2005, MNRAS, 364, L91
Mamajek, E. E., & Meyer, M. R. 2007, ApJ, 668, L175
Marley, M. S., Saumon, D., Guillot, T., Freedman, R. S., Hubbard, W. B., Burrows, A., & Lunine, J. I. 1996, Science, 272, 1919
Marois, C., Lafrenière, D., Doyon, R., Macintosh, B., & Nadeau, D. 2006, ApJ, 641, 556
Marois, C., Macintosh, B., Barman, T., Zuckerman, B., Song, I., Patience, J., Lafrenière, D., & Doyon, R. 2008, Science, 322, 1348
Martin, E. L., & Kun, M. 1996, A&AS, 116, 467
Monet, D. G., et al. 2003, AJ, 125, 984
Moór, A., Ábrahám, P., Derekas, A., Kiss, C., Kiss, L. L., Apai, D., Grady, C., & Henning, T. 2006, ApJ, 644, 525
Nero, D., & Bjorkman, J. E. 2009, ApJ, 702, L163
Oppenheimer, B. R., Kulkarni, S. R., Matthews, K., & Nakajima, T. 1995, Science, 270, 1478
Pollack, J. B., Hubickyj, O., Bodenheimer, P., Lissauer, J. J., Podolak, M., & Greenzweig, Y. 1996, Icarus, 124, 62
Reidemeister, M., Krivov, A. V., Schmidt, T. O. B., Fiedler, S., Müller, S., Löhne, T., & Neuhäuser, R. 2009, A&A, 503, 247
Sadakane, K. 2006, PASJ, 58, 1023
Saumon, D., & Marley, M. S. 2008, ApJ, 689, 1327
Saumon, D., Marley, M. S., Cushing, M. C., Leggett, S. K., Roellig, T. L., Lodders, K., & Freedman, R. S. 2006, ApJ, 647, 552 (S06)
Schröder, C., & Schmitt, J. H. M. M. 2007, A&A, 475, 677
Simons, D. A., & Tokunaga, A. 2002, PASP, 114, 169
Sivanandam, S., Hinz, P. M., Heinze, A. N., Freed, M., & Breuninger, A. H. 2006, Proc., SPIE, 6269, 27
Stephens, D. C., et al. 2009, ApJ, 702, 154
Su, K. Y. L., et al. 2009, ApJ, 705, 314
Tokunaga, A. T., & Vacca, W. D. 2005, PASP, 117, 421
Torres, C. A. O., Quast, G. R., Melo, C. H. F., & Sterzik, M. F. 2008, in Handbook of Star Forming Regions, Vol. II: The Southern Sky, ASP Monograph Publications, Vol. 5, ed. B. Reipurth (San Francisco, CA: ASP), 757
van Leeuwen, F. 2007, A&A, 474, 653
Voges, W., et al. 1999, VizieR Online Data Catalog, 9010, 0
Voges, W., et al. 2000, VizieR Online Data Catalog, 9029, 0
Warren, S. J., et al. 2007, MNRAS, 381, 1400
Wildi, F. P., Brusa, G., Riccardi, A., Lloyd-Hart, M., Martin, H. M., & Close, L. M. 2003, Proc. SPIE, 4839, 155
Williams, J. P., & Andrews, S. M. 2006, ApJ, 653, 1480
Zacharias, N., Monet, D. G., Levine, S. E., Urban, S. E., Gaume, R., & Wycoff, G. L. 2005, VizieR Online Data Catalog, 1297, 0
Zacharias, N., Urban, S. E., Zacharias, M. I., Wycoff, G. L., Hall, D. M., Germain, M. E., Holdenried, E. R., & Winter, L. 2003, VizieR Online Data Catalog, 1289, 0
Zerbi, F. M., et al. 1999, MNRAS, 303, 275
Zuckerman, B., & Song, I. 2004, ARA&A, 42, 685